UWB Radar Imaging based Multipath Delay Prediction for NLOS Position Estimation

Heinrich Luecken and Armin Wittneben
Communication Technology Laboratory, ETH Zurich, 8092 Zurich, Switzerland
{lueckenh, wittneben}@nari.ee.ethz.ch

***Abstract*—Conventional Time-of-Arrival (ToA) based Ultra-Wideband (UWB) positioning suffers strongly from multipath. Harsh propagation environments or non-line-of-sight (NLOS) situations lead to biased position estimates with high estimation errors. To overcome this problem, we propose a radar imaging based method to predict delays of dominant propagation paths. This is done in a three-step approach: First, a radar image of the environment is created using measured training data. We generate a scattering coefficient map with the large synthetic aperture of distributed and moving antennas. The training data can easily be obtained from channel estimates of a UWB communication system with mobile nodes. Second, the radar image is used to reconstruct path gains and path delays. Thus, the channel response is predicted for arbitrary transmitter and receiver positions. Finally, dominant multipath delays are extracted using WRELAX. The proposed algorithm is validated by anechoic chamber measurements with controlled reflectors. Moreover, an extensive measurement campaign in a laboratory/office environment shows that strong paths can be predicted with nanosecond accuracy in a real world scenario.**

I. Introduction

Localization based on Ultra-Wideband (UWB) technology is well investigated and generally considered as method of choice to facilitate high definition positioning [1], [2]. Short-range systems, such as wireless sensor networks (WSN) or wireless body area networks (WBAN) become location aware with UWB. This enables pioneering applications from robotics and industrial automation to the area of healthcare or entertainment [3]. The very high bandwidth of UWB enables centimeter accuracy even under stringent requirements on complexity, costs and energy consumption.

Generally, UWB positioning can be classified into geometric approaches and fingerprinting based systems. Geometric approaches include positioning based on time-of-arrival (ToA) or angle-of-arrival (AoA) determination. The position estimation of a mobile argent node relies on fixed anchor nodes with known positions. For the case of ToA position estimation, the ranges between an agent and several anchors are measured [4]. The individual ranges can then be used to determine the agent position by multilateration [5].

Fingerprinting based systems use location specific features of the propagation channel to determine the agent's position. Usually, a set of measured data with known positions is used as training data. The choice of the fingerprint depends on the training data and the hardware, e.g. system complexity. Promising approaches estimate or classify the agent's position based on extracted signal metrics such as signal strength (RSSI) [6] or the shape of the channel impulse response [7], [8]. However, the performance of location fingerprinting techniques depends on the accuracy of the training data. Conventionally, the positioning error is in the order of the distances of the training samples. Therefore, for high definition positioning, the number of required training samples grows large, which is expensive and impractical to obtain.

While fingerprinting techniques may gain from strong multipath, this is not the case for geometric approaches. In fact, the performance of ToA estimation degrades tremendously in harsh propagation environments. The reason for this is that the line-of-sight (LOS) path may not be distinguishable from multipath or may even not exist. This leads to high position estimation errors and biased results, when no *a priori* channel knowledge is available. Considering the Cramér-Rao lower bound for the unbiased position estimate as presented in [9], we observe that the squared position error even diverges when the separation of overlapping paths goes to zero.

In this paper, we present a method to obtain *a priori* knowledge of multipath delays. We introduce multipath prediction based on a radar image of the environment. Knowledge of multipath delays is of great benefit for geometric as well as fingerprinting based position estimation approaches. Considering ToA estimation, it helps to identify the LOS path and makes position estimation robust against multipath. For fingerprinting methods, multipath prediction can be used to efficiently interpolate between training samples and thus increase accuracy substantially.

The multipath delay prediction makes use of UWB radar imaging techniques with distributed transmit and receive antennas. In a first step, a synthetic aperture radar image of the environment is generated based on training data. We use channel estimates measured at different receiver and transmitter positions as training data, which can be obtained from a UWB communication network with mobile nodes without additional costs. We propose to use a low complexity imaging algorithm to create a map of the scattering coefficients for the area of interest. This map gives information about the location and shape of strong reflectors and scatterers. The second step enables reconstruction of channel responses for arbitrary transmitter and receiver positions. The predicted channel response of new positions is synthesized from the radar image. Finally, we use WRELAX [10] to extract the dominant multipath delays of the predicted channel response. The contribution of this paper can be summarized as follows:

- We provide an algorithm to predict multipath delays for arbitrary transmitter and receiver positions.
- We exploit synergies of UWB imaging and localization. Sensing of the environment is used to improve position estimation by channel response reconstruction.
- The imaging and reconstruction algorithm is validated with anechoic chamber measurements with controlled reflectors.
- The performance of the presented method is evaluated based on an extensive measurement campaign in a laboratory/office environment.

Related work: UWB imaging is used as a basis for the multipath delay prediction. An overview on UWB imaging is given in [11] and [12]. Different migration techniques to generate a UWB short-range image of the environment are described and compared in [13]. To the best of the authors' knowledge, joint UWB imaging and localization has so far not been considered in literature. In [14], simultaneous mapping and localization with an UWB antenna array is presented. This approach relies on extracted features like walls, edges and corners and is not used to facilitate high definition positioning. In [15], UWB position estimation with floor plan information is investigated. However, in this case, a priori knowledge of the propagation environment is necessary and the presence of strong reflectors is required.

The remainder of the paper is structured as follows. Section II describes the system model and in Section III the imaging method to generate the scattering coefficient map is presented. The algorithm for channel response prediction is introduced in Section IV. Finally, in Section V the performance of the presented scheme is evaluated for an indoor environment and conclusions are drawn in Section VI.

II. System Setup and Problem Formulation

We consider a network with two types of UWB communication nodes, which are referred to as anchor nodes and agent nodes. The anchor nodes are stationary and their absolute position is known with high accuracy. Agent nodes are mobile and usually subject to position estimation. Here, we want to predict the multipath conditions for arbitrary agent positions.

Considering radio transmission from agent to anchors, the receive signal is modeled by

$$r(t) = \sum_{n=0}^{L} \gamma_n s(t-\tau_n) + w(t),$$

where $s(t)$ and $w(t)$ denote transmit signal and noise, respectively. The smallest path delay τ_n corresponds to the LOS path and dominant propagation paths are characterized by large path gains γ_n. We denote the receive signal correlated with the transmit signal $s(t)$ as channel response $\psi(t)$, where $s(t)$ preferably has a flat spectrum in the considered bandwidth.

The channel response depends on the position of the transmitting agent as well as on the position of the receiving anchor. Suppose an agent is moved though the coverage area of the considered network and the anchor nodes successively record channel responses. In combination with the position information of the anchor and agents, this forms a training data set. The training data set $\mathcal{M}$ is defined as

$$\mathcal{M} = \left\{ \psi^{(1)}(t), \mathbf{p}_{\text{tx}}^{(1)}, \mathbf{p}_{\text{rx}}^{(1)}, \ldots, \psi^{(N)}(t), \mathbf{p}_{\text{tx}}^{(N)}, \mathbf{p}_{\text{rx}}^{(N)} \right\},$$

where $\psi^{(k)}(t)$, $\mathbf{p}_{\text{tx}}^{(k)} = [x_{\text{tx}}^{(k)}, y_{\text{tx}}^{(k)}]^T$, $\mathbf{p}_{\text{rx}}^{(k)} = [x_{\text{rx}}^{(k)}, y_{\text{rx}}^{(k)}]^T$ denote channel response, transmitter position and receiver position for measurement number $k = 1, \ldots, N$, respectively. Given the data set $\mathcal{M}$, we want to find the delays of the dominant paths for an arbitrary agent position $\mathbf{p}_{\text{tx}}$ and anchor position $\mathbf{p}_{\text{rx}}$. We assume a static environment and a constant velocity medium with propagation speed $c = c_0$, the speed of light in vacuum.

III. Scattering Coefficient Map of Environment

To generate an image of the environment we use synthetic aperture processing. We estimate the scattering coefficient $\hat{\alpha}_{\mathcal{M}}(\mathbf{r})$ for every point $\mathbf{r}$ in the coverage area of the considered network. The reconstruction algorithm is given by

$$\hat{\alpha}_{\mathcal{M}}(\mathbf{r}) = \frac{1}{N} \sum_{k=1}^{N} R_1^{(k)}(\mathbf{r}) R_2^{(k)}(\mathbf{r}) \cdot \psi^{(k)} \left(\frac{R_1^{(k)}(\mathbf{r}) + R_2^{(k)}(\mathbf{r})}{c} \right), \tag{1}$$

where $R_1^{(k)}(\mathbf{r})$ and $R_2^{(k)}(\mathbf{r})$ correspond to the distance between point $\mathbf{r}$ and agent and anchor, respectively. In the following, we consider the 2D case, i.e. $\mathbf{r} = [x, y]^T$. The distances are then given by

$$R_1^{(k)}(x,y) = \sqrt{\left(x - x_{\text{tx}}^{(k)}\right)^2 + \left(y - y_{\text{tx}}^{(k)}\right)^2}$$

and

$$R_2^{(k)}(x,y) = \sqrt{\left(x - x_{\text{rx}}^{(k)}\right)^2 + \left(y - y_{\text{rx}}^{(k)}\right)^2}.$$

The principle of the imaging algorithm is that each point $\mathbf{r}_1 = [x_1, y_1]^T$ in the coverage area can be mapped to a delay in the channel responses. This delay depends on the agent and anchor positions and is determined by $\frac{1}{c}(R_1^{(k)}(\mathbf{r}_1) + R_2^{(k)}(\mathbf{r}_1))$. If we average now over many agent positions, path gains add up coherently in case of a reflector or scatterer and average out, if no object is present. To compensate the effect of path-loss, the channel response is scaled by the distances of the considered point to the transmitter and receiver. Hence, we asymptotically obtain a map of intensity and location of reflectors and scatterers. Note that the LOS component in the channel response does not correspond to a reflector or scatterer. Therefore, we substitute the LOS part of the channel responses $\psi^{(k)}(t)$ by zeros before generating the scattering coefficient map according to (1).

In geophysics and seismology, equation (1) is known as diffraction summation migration [16]. It is straightforward to extend the presented multipath delay prediction algorithm by other imaging techniques, such as Kirchhoff migration or finite difference methods for wave propagation and migration [17]. However, we omit this due to computational complexity,

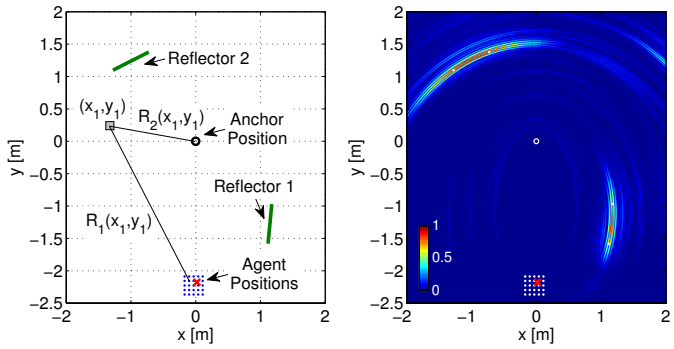

Fig. 1. Anechoic chamber measurements with two reflectors: setup (left) and magnitude of scattering coefficient map (right)

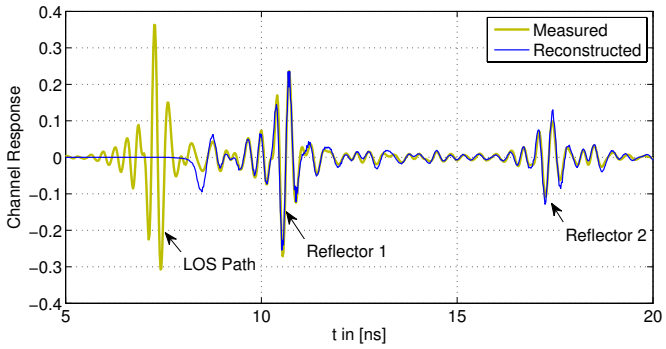

Fig. 2. Reconstructed and measured channel response of controlled anechoic chamber environment with two reflectors

the distributed transmit and receive antenna and non-uniform measurement steps.

Fig. 1 shows the result of the imaging algorithm for a controlled environment in an anechoic chamber with two metallic reflectors. The left hand side depicts the position of reflectors, anchor and agent. Channel responses have been measured in the bandwidth from 2 to 6 GHz, while the agent was moved on a horizontal 1 cm grid over an area of 0.28 cm $\times$ 0.28 cm. The measurement setup and successive postprocessing is described in detail in [18]. The right hand side of Fig. 1 shows the magnitude of the scattering coefficient map according to (1) based on $N = 840$ channel responses. The position and intensity of the two reflectors can be clearly determined.

IV. Channel Response Prediction

So far, we have extrapolated the time domain channel responses to the spatial dimension by generating a scattering coefficient map. Next, the spatial data is transformed to a channel response. The knowledge of the propagation environment enables to predict the channel response for an arbitrary position. This is done by synthesizing the channel response from the scattering coefficients with the corresponding delays. The predicted channel response $\hat{\Psi}_{\mathbf{p}_{\text{tx}},\mathbf{p}_{\text{rx}}}(f)$ in frequency domain with new transmitter and receiver position $\mathbf{p}_{\text{tx}} = [x_{\text{tx}}, y_{\text{tx}}]^T$ and $\mathbf{p}_{\text{rx}} = [x_{\text{rx}}, y_{\text{rx}}]^T$ is given by:

$$\hat{\Psi}_{\mathbf{p}_{\text{tx}},\mathbf{p}_{\text{rx}}}(f) = \int_x \int_y \frac{\hat{\alpha}_{\mathcal{M}}(x,y) e^{-j2\pi f \frac{R_1(x,y)+R_2(x,y)}{c}}}{R_1(x,y)R_2(x,y)} dxdy, \tag{2}$$

where $R_1(x,y)$ and $R_2(x,y)$ are the distances between $[x,y]^T$ and $\mathbf{p}_{\text{tx}}$ and $\mathbf{p}_{\text{rx}}$, respectively. The delay of a scatterer at position $[x,y]^T$ with intensity $\hat{\alpha}_{\mathcal{M}}(x,y)$ leads to a phase shift depending on the distance to the receiver and transmitter position. The path loss is incorporated by appropriate scaling with the distance.

Finally, the dominant multipath components are extracted from $\hat{\Psi}_{\mathbf{p}_{\text{tx}},\mathbf{p}_{\text{rx}}}(f)$. This gives an estimate of the multipath delays as a function of the agent and anchor position. The $\tilde{L}$-strongest predicted multipath delays $\hat{\tau}_l$ are obtained by

$$(\hat{\tau}_1, \ldots, \hat{\tau}_{\tilde{L}}) = \underset{\substack{\tilde{\gamma}_1,\ldots,\tilde{\gamma}_{\tilde{L}} \\ \tilde{\tau}_1,\ldots,\tilde{\tau}_{\tilde{L}}}}{\arg\min} \int_{-\infty}^{\infty} \left| \hat{\Psi}_{\mathbf{p}_{\text{tx}},\mathbf{p}_{\text{rx}}}(f) - |S(f)|^2 \sum_{n=1}^{\tilde{L}} \tilde{\gamma}_l e^{-j2\pi f \tilde{\tau}_l} \right|^2 df,$$

where $S(f)$ denotes the Fourier transform of the transmit signal $s(t)$. We propose to solve the optimization problem with WRELAX, see [10].

For the sake of computational complexity, we introduce sampling of the scattering coefficient map with spacing Δx and Δy and of the channel response with a sampling frequency f_s. In discrete time, the channel response prediction (2) can then be approximated by

$$\hat{\psi}_{\mathbf{p}_{\text{tx}},\mathbf{p}_{\text{rx}}}[k] = \sum_l \sum_m \frac{\hat{\alpha}_{\mathcal{M}}(x_l,y_m)\Delta x \Delta y}{R_1(x_l,y_m)R_2(x_l,y_m)} \cdot \delta\left[k - \tfrac{f_s}{c}(R_1(x_l,y_m) + R_2(x_l,y_m))\right]$$

where $\delta[\cdot]$ denotes the Kronecker delta with the argument rounded to the nearest integer.

Fig. 2 shows a reconstructed channel response from the controlled anechoic chamber environment. The channel response corresponds to agent position $[0.018\text{ m}, -2.177\text{ m}]^T$, which is marked by a red cross in Fig. 1. Additionally, the measured channel response at this position is plotted. Note that the measured channel response has not been used for the reconstruction, i.e. it was excluded from the training set to generate the scattering coefficient map. The reconstructed and the measured channel response fit very well. The reconstructed channel response does not contain the LOS path, since it does not originate from reflection or scattering.

V. Performance Evaluation

To evaluate the proposed algorithm in a typical indoor environment, we performed an extensive measurement campaign with one mobile agent node and four stationary anchors. Fig. 3 depicts the measurement setup schematically. The agent periodically transmits a 3.27 μs long pseudo-noise sequence in

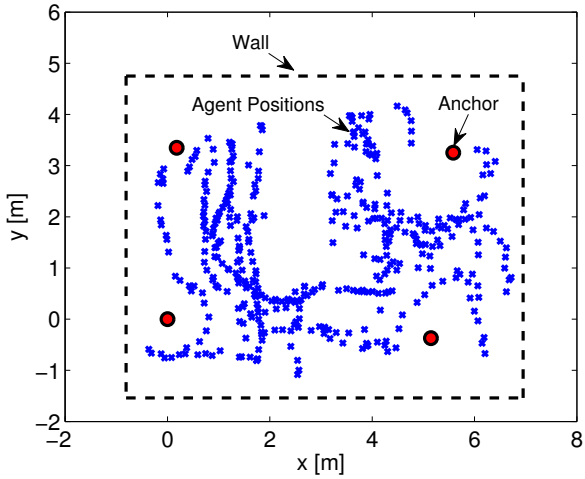

Fig. 4. Measurement positions and coarse floor plan of environment

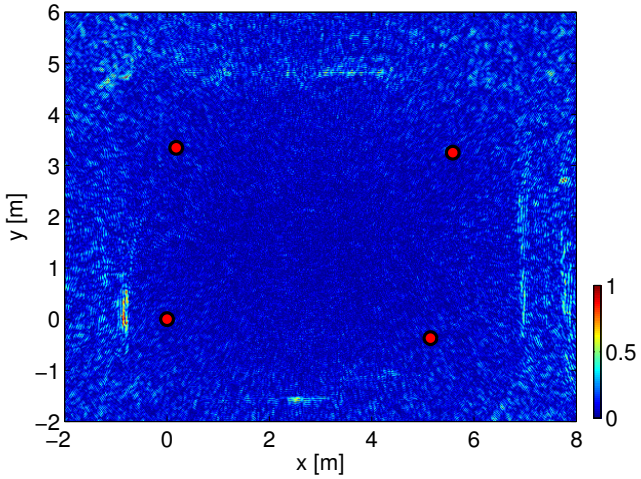

Fig. 5. Laboratory environment: Magnitude of scattering coefficient map

the frequency band from approximately 2 to 6 GHz. The signal is generated by an arbitrary waveform generator, amplified by 30 dB and transmitted over an antenna. The agent as well as the anchors use Skycross SM3TO10MA antennas, which were mounted at a height of 1.85 m. The antennas have approximately omnidirectional gain in azimuth. At the anchors, the receive signal is amplified by low noise amplifiers and recorded by a digital sampling oscilloscope. The anchors are synchronized to the agent by cable using an external trigger.

Fig. 4 shows an approximate floor plan of the laboratory where the measurements took place. Additionally, the anchor and agent positions are plotted. The agent was manually moved to 400 different positions and the corresponding channel response to the four anchors has been measured. The total number of measured channel responses is therefore $N = 1600$. The channel responses have an estimated signal-to-noise-ratio of approximately 70 dB. In Fig. 5, the magnitude of the scattering coefficient map according to (1) is plotted. In this environment, the reflectors are not as strong and well defined as in the anechoic chamber with metallic reflectors. However, the walls of the room can be recognized from the image. The image is sampled with a spacing of $\Delta x = 2$ cm and $\Delta y = 1.6$ cm. In time domain, the sampling frequency has been chosen to $f_s = 50$ GHz.

Fig. 6 shows the measured (top) as well as reconstructed (bottom) channel response for one anchor position. The measured channel response was excluded from training data for the reconstruction. Note that the reconstructed channel response contains out-of-band noise, which does not perturb the multipath delay estimation. Hence, we plot also the five strongest paths of both channel responses, which are extracted by WRELAX (without LOS path). It can be observed that the multipath delays of strong paths can be predicted with high accuracy.

To evaluate the accuracy of multipath delay prediction more generally, for all 400 agent positions and four different anchors the channel responses have been reconstructed. Each reconstruction was based on the training set excluding the measurements of the considered agent position. Subsequently, the five strongest multipath components have been estimated by WRELAX for the synthesized channel responses as well as for the measurement. Fig. 7 shows the empirical CDF of the prediction error of the multipath delay. Both predicted and measured channel response multipath extraction results in five delays. The pair with the smallest absolute error is denoted as first fit. The evaluation shows that in almost all cases at least one out of the five delays can very accurately

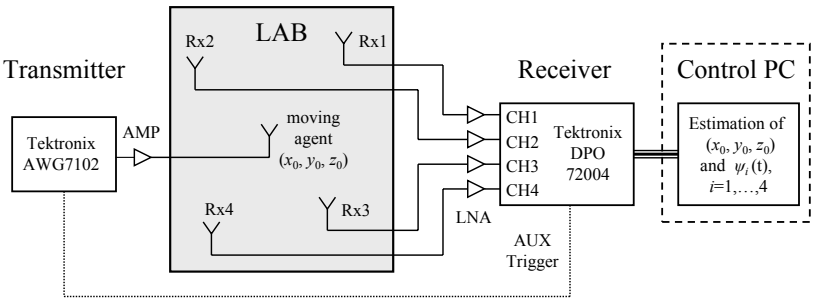

Fig. 3. Schematic diagram of measurement setup and photo of laboratory and measurement equipment

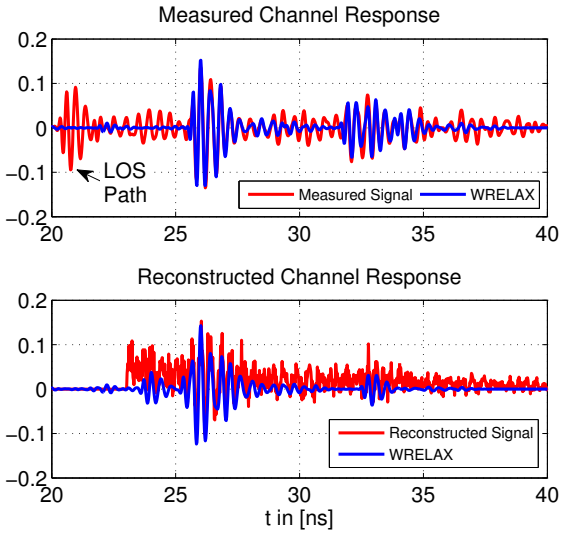

Fig. 6. Measured and reconstructed channel response

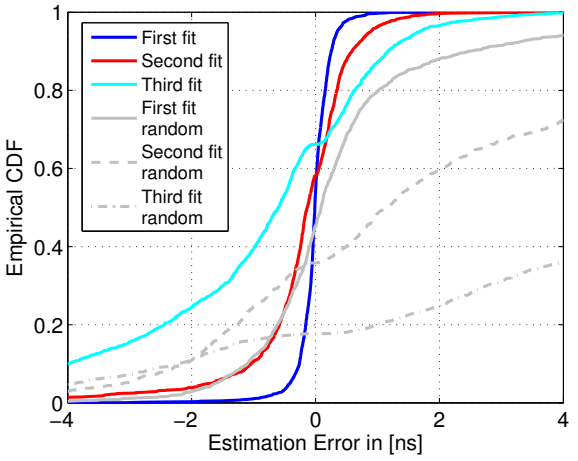

Fig. 7. CDF of path delay estimation error

be predicted with less than 1 ns error. The root mean square error (RMSE) is 0.298 ns. The second fit corresponds to the pair with the smallest absolute error among the remaining four delays. Here, we observe in 85.6% an absolute error below 1 ns and accordingly for the third fit still in 47.7% of the agents positions. For comparison, we plot the first, second and third fit of five randomly generated multipath delays, which are uniformly distributed in the interval $[t_{\mathrm{ToA}}, t_{\mathrm{ToA}} + 39.48 \text{ ns}]$. The time t_{ToA} denotes the time-of-arrival of the LOS path and 39.48 ns corresponds to the maximal detected excess delay of the measured channel responses. Here, the RMSE of the first fit evaluates to 2.093 ns, which is almost an order of magnitude worse than the proposed algorithm.

VI. Conclusions

In this paper, we have proposed to predict multipath delays with UWB imaging. Based on measured training data an image of the environment is generated. The image describes position and intensity of strong scatterers and reflectors. With this information, the strong multipath components can be predicted for arbitrary transmitter and receiver positions. Performance evaluation based on a controlled anechoic chamber environment as well as an indoor environment prove the feasibility of the presented approach. Strong multipath can be predicted within nanoseconds accuracy. Considering UWB localization, synergies with short-range imaging can be used to facilitate high definition positioning.

Acknowledgment

The authors would like thank Christoph Steiner for providing the anechoic chamber measurements.

References

[1] S. Gezici and H. Poor, "Position estimation via ultra-wide-band signals," *Proceedings of the IEEE*, vol. 97, no. 2, pp. 386–403, Feb. 2009.

[2] K. Pahlavan, X. Li, and J. Makela, "Indoor geolocation science and technology," *IEEE Communications Magazine*, vol. 40, no. 2, pp. 112–118, Feb. 2002.

[3] Z. Mekonnen, E. Slottke, H. Luecken, C. Steiner, and A. Wittneben, "Constrained maximum likelihood positioning for UWB based human motion tracking," in *International Conference on Indoor Positioning and Indoor Navigation, IPIN 2010*, Sept. 2010.

[4] D. Dardari, A. Conti, U. Ferner, A. Giorgetti, and M. Win, "Ranging with ultrawide bandwidth signals in multipath environments," *Proceedings of the IEEE*, vol. 97, no. 2, pp. 404–426, Feb. 2009.

[5] W. Foy, "Position-location solutions by taylor-series estimation," *IEEE Transactions on Aerospace and Electronic Systems*, vol. AES-12, no. 2, pp. 187–194, 1976.

[6] P. Bahl and V. Padmanabhan, "RADAR: an in-building RF-based user location and tracking system," in *Nineteenth Annual Joint Conference of the IEEE Computer and Communications Societies, INFOCOM 2000*, vol. 2, Mar. 2000, pp. 775–784.

[7] C. Steiner, F. Althaus, F. Troesch, and A. Wittneben, "Ultra-wideband geo-regioning: A novel clustering and localization technique," *Eurasip Journal on Advances in Signal Processing*, November 2007.

[8] C. Steiner and A. Wittneben, "Low complexity location fingerprinting with generalized UWB energy detection receivers," *IEEE Transactions on Signal Processing*, vol. 58, no. 3, pp. 1756 –1767, 2010.

[9] Y. Shen and M. Win, "Fundamental limits of wideband localization – Part I: A general framework," *IEEE Transactions on Information Theory*, vol. 56, no. 10, pp. 4956–4980, 2010.

[10] J. Li and R. Wu, "An efficient algorithm for time delay estimation," *IEEE Transactions on Signal Processing*, vol. 46, no. 8, pp. 2231–2235, Aug. 1998.

[11] R. Zetik, J. Sachs, and R. Thoma, "UWB short-range radar sensing - the architecture of a baseband, pseudo-noise UWB radar sensor," *IEEE Instrumentation Measurement Magazine*, vol. 10, no. 2, pp. 39–45, 2007.

[12] L. Jofre, A. Broquetas, J. Romeu, S. Blanch, A. Toda, X. Fabregas, and A. Cardama, "UWB tomographic radar imaging of penetrable and impenetrable objects," *Proceedings of the IEEE*, vol. 97, no. 2, pp. 451–464, 2009.

[13] X. Zhuge, T. Savelyev, A. Yarovoy, L. Ligthart, and B. Levitas, "Comparison of different migration techniques for UWB short-range imaging," in *European Radar Conference, EuRAD 2009*, Oct. 2009, pp. 184–187.

[14] T. Deissler and J. Thielecke, "Feature based indoor mapping using a bat-type UWB radar," in *IEEE International Conference on Ultra-Wideband, ICUWB 2009*, Sept. 2009, pp. 475–479.

[15] P. Meissner, C. Steiner, and K. Witrisal, "UWB positioning with virtual anchors and floor plan information," in *7th Workshop on Positioning Navigation and Communication, WPNC 2010*, 2010, pp. 150–156.

[16] J. Gazdag and P. Sguazzero, "Migration of seismic data," *Proceedings of the IEEE*, vol. 72, no. 10, pp. 1302–1315, Oct. 1984.

[17] J. A. Scales, *Theory of Seismic Imaging*. Springer-Verlag Berlin Heidelberg, 1995.

[18] C. Steiner, "Location fingerprinting for ultra-wideband systems - the key to efficient and robust localization," Ph.D. dissertation, PhD Thesis, 2010.